

Direct Numerical Simulations of Centrifugal Buoyancy Induced Flow in a Closed Rotating Cavity

Deepak Saini, Daniel Chung, Richard D. Sandberg

Department of Mechanical Engineering
 The University of Melbourne, Victoria 3010, Australia

Abstract

The present study is a numerical investigation of buoyancy-induced flow in a rapidly rotating system. This problem is relevant to planetary flows in the atmosphere as well as to rotating machinery such as gas turbine, where rapid rotation and temperature gradients lead to convection induced by the centrifugal force. We solve the compressible Navier–Stokes equations in an inertial frame of reference to study the flow for Rayleigh numbers in the range of 10^6 to 10^8 . The prediction of heat transfer shows good agreement with experimental data. Visualisations show the formation of counter-rotating convection cells, analogous to Rayleigh–Bénard convection. The present predictions are also compared with simulations which solve the incompressible equations using the Boussinesq approximation, which shows the overprediction of temperature gradient and consequently the overprediction of the averaged Nusselt number compare to the results of the present study. The qualitative comparison of density distribution is also reported in this study.

Introduction

Centrifugal buoyancy induced flow occurs in rapidly rotating systems where the centrifugal force dominates over other body forces and the fluid motion is generated by density differences. This problem is relevant to planetary flows in the atmosphere as well as to the internal air system of gas turbines. This study focuses on the latter in the cavities between the compressor disks of a gas turbine. Although the actual geometry is quite complex, in this study, a simplified model is used to understand the flow physics and heat transfer near operating conditions. Figure 1 shows the schematic of the annular rotating cavity used in this study. The annular cavity is bounded between two insulated side disks, and an outer cylindrical surface at high temperature and an inner cylindrical surface at low temperature. This imposed radial temperature difference creates radial density difference across the cavity. This density difference combined with the centrifugal force due to the rotation induces fluid flow in the cavity relative to solid body rotation.

Initial experiments for the closed rotating cavity were carried out by Bohn et al. [1]. They reported results for annular cavities with radial inward heat flux. Average Nusselt number data were presented for the different values of rotational Rayleigh number. An empirical correlation between Nusselt number (Nu) and rotational Rayleigh number (Ra) was found as $Nu = 0.317Ra^{0.211}$. However, the experiments were designed to measure the heat transfer only, and consequently no information about the flow structure was reported. A pioneering numerical study by Sun et al. [9] investigated the closed cavity problem by solving compressible Navier–Stokes equations in a 45° azimuthal sector of the full cavity for the same configuration as [1] and predicted the Nusselt number in good agreement with the experimental results. Further analysis concluded the presence of large-scale structures in the cavity which lead to the significant variation of the average heat transfer rate from the wall. Another numerical study by King et al. [4], in which the 2D Navier–Stokes equations were solved using a vorticity-

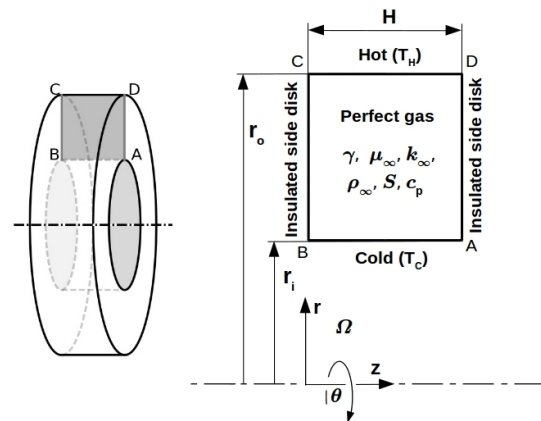


Figure 1: Schematic of closed annular cavity. The walls of the cavity undergo solid-body rotation about the z -axis.

stream function approach, also found flow structure analogous to Rayleigh–Bénard convection. The Nusselt number computed at the outer wall was also shown to be in good agreement with the results of Rayleigh–Bénard convection, which was significantly higher than the measurements of Bohn et al. [1]. A DNS study by Pitz et al. [7] examined the same cavity configuration by solving 3D unsteady incompressible Navier–Stokes equations using the Boussinesq approximation. Large-scale convection rolls (counter-rotating vortices) were observed in the domain. The Nusselt number predicted at the outer wall was observed to be in agreement with the correlation of Hollands et al. [3] for natural convection between two parallel horizontal plates under gravity. A recent LES study by the same authors [6] reported the time and spatially averaged quantities, including mean temperature and velocity fluctuations in the domain for the same cavity configuration. However, in the study [7], authors also tested another variant of the Boussinesq approximation (extended for rotating flows by Lopez et al. [5]), which was reported to be imperfect for this problem as smearing of the flow structures was observed in the azimuthal direction. Interestingly, the Nusselt number scaling for the second variant of the Boussinesq approximation was reported to be in close agreement with experimental results [1] after applying a correction to compensate for the heat loss from the side walls. This apparent conflicting situation requires further investigation by analyzing the problem with a fully compressible formulation that does not rely on the Boussinesq approximation.

Thus the objective of this study is to investigate the centrifugal buoyancy induced flow in a closed rotating cavity at the same conditions as in the experiments by Bohn et al. [1] by solving the compressible Navier–Stokes equations.

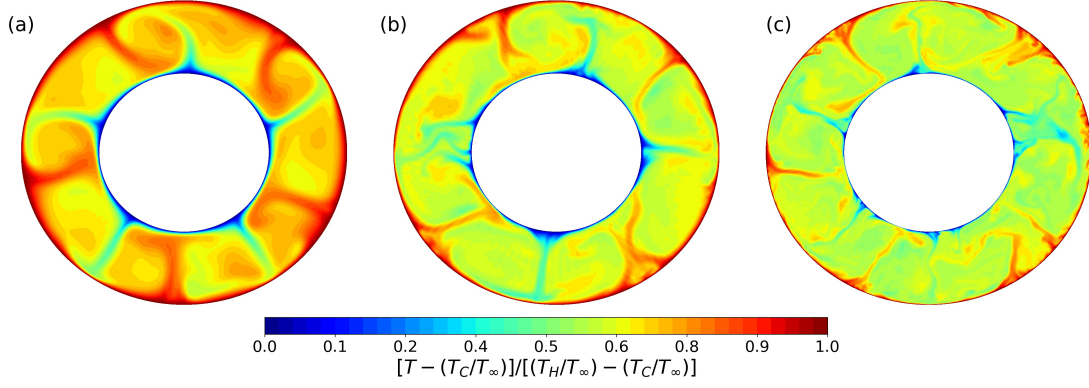


Figure 2: Instantaneous temperature contours at mid-axial position $z = (1/2)(H/r_o)$ of the cavity rotating in the clockwise direction for (a) $Ra = 10^6$, $Re_\infty = 8693$ (b) $Ra = 10^7$, $Re_\infty = 41495$ and (c) $Ra = 10^8$, $Re_\infty = 113012$.

Problem Description and Numerical method

The computational domain is a closed annular cavity that rotates at angular velocity Ω about its axis (figure 1), where r_i and r_o are the inner and outer radii, respectively, and H is the spacing between the side disks of the cavity. The outer wall is hot (temperature T_H) and the inner wall is cold (temperature T_C), i.e. $\Delta T = T_H - T_C > 0$. The cavity is filled with a canonically perfect gas with specific heat at constant pressure c_p and ratio of specific heats γ . At $T_\infty \equiv (T_H + T_C)/2$, the dynamic viscosity is μ_∞ and the thermal conductivity is k_∞ . The compressible Navier–Stokes equations for the conservative variables are solved in an inertial frame, where the mass, momentum and energy equations, non-dimensionalised with velocity Ωr_o , length r_o , density ρ_∞ and pressure $\rho_\infty(\Omega r_o)^2$, are given as

$$\frac{\partial \rho}{\partial t} + \frac{\partial}{\partial x_k}(\rho u_k) = 0, \quad (1)$$

$$\frac{\partial}{\partial t}(\rho u_i) + \frac{\partial}{\partial x_k}[\rho u_i u_k + p \delta_{ik} - \tau_{ik}] = 0, \quad (2)$$

$$\frac{\partial}{\partial t}(\rho E) + \frac{\partial}{\partial x_k}[u_k(\rho E + p) + q_k - u_i \tau_{ik}] = 0, \quad (3)$$

respectively, where the total energy, $E = T/[\gamma(\gamma - 1)M_\infty^2] + (1/2)u_i u_i$ and the equation of state is $p = \rho T/(\gamma M_\infty^2)$. The viscous stress tensor and the heat-flux vector are computed as

$$\tau_{ik} = \frac{\mu}{Re_\infty} \left(\frac{\partial u_i}{\partial x_k} + \frac{\partial u_k}{\partial x_i} - \frac{2}{3} \frac{\partial u_j}{\partial x_j} \delta_{ik} \right), \quad (4)$$

$$q_k = \frac{-\mu}{(\gamma - 1)Ma_\infty^2 Pr_\infty Re_\infty} \frac{\partial T}{\partial x_k}.$$

The shear molecular viscosity is computed using Sutherland's law, $\mu = T^{3/2}(1 + S/T_\infty)/(T + S/T_\infty)$, where S is the Sutherland temperature. The non-dimensional numbers that completely specify this problem are given as

$$Re_\infty \equiv \frac{\rho_\infty(\Omega r_o)r_o}{\mu_\infty}, \quad Pr_\infty \equiv \frac{\mu_\infty c_p}{k_\infty} = 0.71, \quad \gamma = 1.4$$

$$\frac{S}{T_\infty} = 0.368, \quad Ma_\infty \equiv \frac{\Omega r_o}{(c_p(\gamma - 1)T_\infty)^{1/2}} = 0.2, \quad (5)$$

$$\frac{\Delta T}{T_\infty}, \quad \frac{r_i}{r_o} = 0.52, \quad \frac{H}{r_o} = 0.5,$$

where Re_∞ , Pr_∞ and Ma_∞ are the reference Reynolds number, Prandtl number and Mach number, respectively. While (1)-(4) are written in Cartesian coordinates for simplicity, they

are actually solved in cylindrical coordinates with u , v and w representing the non-dimensional velocity components in z , r and θ directions, respectively. The boundary conditions for this problem are thus $u = v = 0$ for all walls of the cavity and, since all walls are rotating at constant angular velocity, $w(z, r = r_i/r_o, \theta) = r_i/r_o$, $w(z, r = 1, \theta) = 1$ and $w(z = 0, r, \theta) = w(z = H/r_o, r, \theta) = r$. The outer and inner cylindrical walls of the cavity are isothermal $T(z, 1, \theta) = T_H/T_\infty = 1 + (1/2)\Delta T/T_\infty$ and $T(z, r_i/r_o, \theta) = T_C/T_\infty = 1 - (1/2)\Delta T/T_\infty$. The side disks of the cavity are insulated so that $q_z = 0 \Rightarrow \partial T/\partial z = 0$ on both side disks. In this study, the effect of gravity is neglected as the centrifugal force is much larger than the gravitational force ($\Omega^2 r_o/g \gg 1$).

The code HiPSTAR (High Performance Solver for Turbulence and Aeroacoustics Research) [8] is used, where the axial (z) and radial (r) directions are discretised with a fourth-order accurate finite-difference scheme and the azimuthal (θ) direction is discretised with a Fourier spectral method. Time integration is achieved using a low-storage fourth-order accurate Runge–Kutta scheme. The code has been validated with DNS of Taylor–Couette flow [2] and comparison of the mean azimuthal velocity profile shows good agreement with a maximum error of 5%.

It is customary in natural convection problem to define the Rayleigh and Nusselt numbers [1]:

$$Ra \equiv \frac{[\Omega^2(r_o + r_i)/2](\Delta T/T_\infty)(r_o - r_i)^3}{(\mu_\infty/\rho_\infty)(k_\infty/\rho_\infty c_p)} \quad (6)$$

$$= Re_\infty^2 Pr_\infty \frac{\Delta T}{T_\infty} \frac{1}{2} \left(1 + \frac{r_i}{r_o}\right) \left(1 - \frac{r_i}{r_o}\right)^3,$$

$$Nu \equiv \frac{q_{convection}}{q_{conduction}} = \frac{\ln(r_o/r_i)}{\Delta T/T_\infty} \left[\mu \frac{dT}{dr} \right]_{r=1}, \quad (7)$$

characterising the driving and response of the system. A more representative Mach number is based on the free-fall velocity $u_f^2 \equiv [\Omega^2(r_o + r_i)/2](\Delta T/T_\infty)(r_o - r_i)$:

$$Ma_f \equiv \frac{u_f}{(c_p(\gamma - 1)T_\infty)^{1/2}} = Ma_\infty \left[\frac{\Delta T}{T_\infty} \frac{1}{2} \left(1 - \frac{r_i^2}{r_o^2}\right) \right]^{1/2}. \quad (8)$$

These can be related to the quantities in (5) via $Ra = 0.05944 \cdot Re_\infty^2 (\Delta T/T_\infty)$ and $Ma_f = 0.6036 \cdot Ma_\infty (\Delta T/T_\infty)^{1/2}$. For reference, $Re_\infty = Ek^{-1}$, the inverse Ekman number and the inverse Rossby number, $Ro^{-1} \equiv 2\Omega(r_o - r_i)/u_f = 2^{3/2}(1 - r_i/r_o)^{1/2}(1 + r_i/r_o)^{-1/2}(\Delta T/T_\infty)^{-1/2}$, which simplifies to $Ro^{-1} = 1.587 \cdot (\Delta T/T_\infty)^{-1/2}$. In the compressor cavities

of a gas turbine, typical Ra , Re_∞ and Ma_∞ , are of the order 10^{12} , 10^6 and 0.4, respectively.

Results and Discussion

Direct numerical simulations have been carried out for Rayleigh numbers in the range $10^6 < Ra < 10^8$ (table 1) for the full circumferential domain size of 360° degrees (figure 1).

Case	Re_∞	$\Delta T/T_\infty$	Ra	Ma_f	$N_r \times N_z \times N_\theta$	Nu
1	8693	0.24	10^6	0.059	$160 \times 160 \times 194$	6.15
2	41400	0.12	10^7	0.038	$200 \times 200 \times 194$	10.3
3	113012	0.13	10^8	0.043	$432 \times 432 \times 258$	23.5

Table 1: DNS cases: N_r , N_z and N_θ are number of grid points in respective directions.

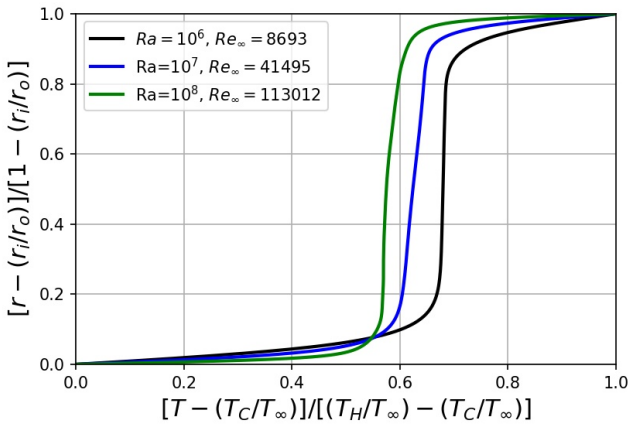


Figure 3: Comparison of average temperature profiles at different Rayleigh numbers. The temperature profiles are averaged over $(1/4)(H/r_o) \leq z/r_o \leq (3/4)(H/r_o)$ to be consistent with [6].

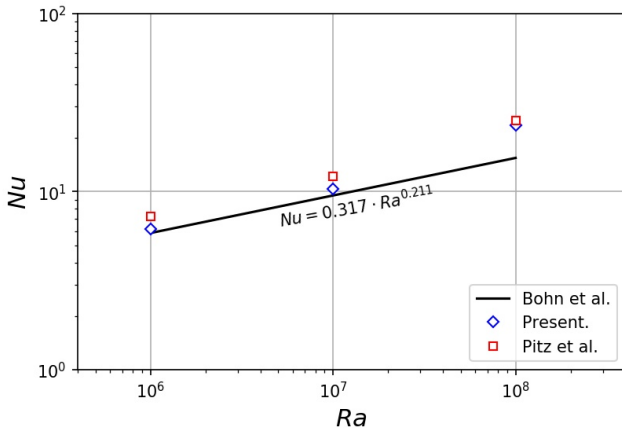


Figure 4: Comparison of Nusselt number Scaling with Rayleigh with the scaling reported by Bohn et al.[1], Pitz et al.[7].

Figure 2 shows the instantaneous temperature contours in the $r - z$ plane at the mid-axial position of a cavity rotating in the clockwise direction. The flow structures consist of counter-rotating vortices that continuously transport hot fluid from the outer wall to the inner wall and cold fluid from the inner to the outer wall. This phenomenon is analogous to Rayleigh-Bénard convection in which similar counter-rotating vortices form between two parallel plates at different temperature levels under

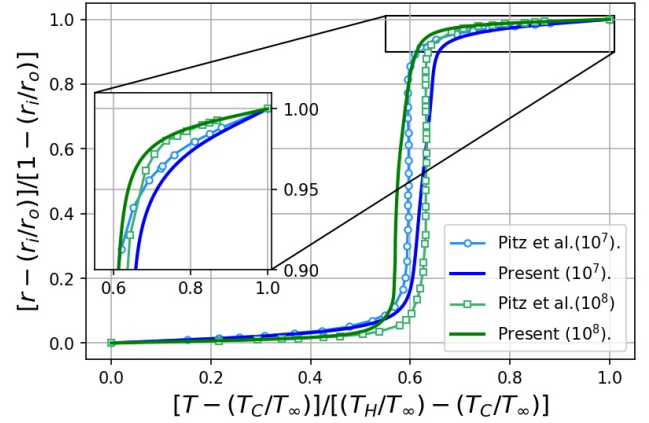


Figure 5: Comparison of average temperature profiles with the results reported by Pitz et al.[6]. The temperature profiles are averaged over $(1/4)(H/r_o) \leq z/r_o \leq (3/4)(H/r_o)$ to be consistent with [6].

a gravitational force field. The flow pattern is discernible with the formation of mushroom-shaped plume structures in the cavity. However, at higher Ra of 10^7 and 10^8 , turbulence leads to a break-down of the symmetrical structures and leads to more temperature uniformity in the core region. The number of large identifiable structures is five for low Ra of 10^6 and is reduced to four for Ra of 10^7 and again increases to five cells for Ra of 10^8 . Figure 3 shows the temperature profile averaged over time, circumferential and axial direction for different Ra . The bulk has almost uniform temperature with large gradients only near the boundary. With the increase in the Ra , the extent of bulk is increasing with the rise in the temperature gradient near the walls of the cavity. A temperature drop in the core region is observed with the increase in the Ra , which can be inferred from Fig. 2 as well; as more mixing in the core region at high Ra leads to drop in the average temperature of the bulk.

Figure 4 presents the Nu , which characterizes the heat-transfer efficiency. The comparison shows a good overall agreement of Nusselt number at the outer wall with the experimental correlation [1]. A deviation of 3% and 5% in Nu is observed with respect to the experiments for $Ra = 10^6$ and 10^7 respectively. This is well within experimental error range reported in [1], due to the imperfect insulation of the side walls in the experiments. However, a larger deviation is observed for $Ra = 10^8$. Further, DNS results using an incompressible, Boussinesq approximation [7] shows a higher Nu . Figure 5 presents the comparison of the averaged temperature profile with LES [6]. The comparison shows the prediction of the higher temperature gradient in the radial direction for the $Ra = 10^7$ near the outer wall compare to the results of the present study. This can be directly related to the overprediction of Nu at the outer wall as shown in Fig. 4. However, in the case of $Ra = 10^8$, the near wall temperature profile looks identical, which is consistent with the prediction of Nu as shown in Fig. 4. However, a large deviation is observed in the temperature of the core region of the cavity for both the Ra . Further, as reported by Pitz et al.[6] and shown in Fig. 5, the core temperature increases with the increase in the Ra . This trend is opposite to the results of the current study as shown in Fig. 3, where the core temperature decreases with the increase in the Rayleigh number.

The reason for the deviation in the temperature profile near the wall and consequent overprediction of the Nusselt number may be due to the assumption of density as a linear function of temperature in the Boussinesq approximation. This can be proved qualitatively by comparing the density distribution in the do-

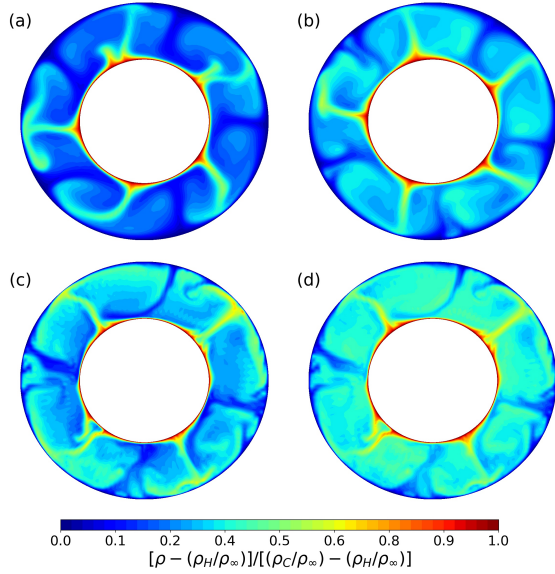


Figure 6: Instantaneous density contours at mid-axial position $z = (1/2)(H/r_o)$ of the cavity for (a) $Ra = 10^6$ obtained compressible code results, (b) $Ra = 10^6$ from linear approximation, (c) $Ra = 10^7$ obtained compressible code results and (d) $Ra = 10^7$ from linear approximation.

main calculated from the same instantaneous temperature field. Figure 6 shows the instantaneous density distribution obtained directly from the compressible formulation and calculated by using the algebraic expression of the Boussinesq approximation $[\rho = \rho_\infty(1 - (T - 1))]$ applied to the same instantaneous temperature field of compressible DNS. The results show that the density contours obtained from compressible calculations as shown in Fig. 6a and 6c for the $Ra = 10^6$ and 10^7 , respectively, are quite different from the ones obtained from the linear approximation of density shown in Fig. 6b and 6d for the same Ra . As observed from the instantaneous density contours of compressible formulation, most of the core region of the cavity is filled with the less dense or hot fluid from the outer wall with the narrow plumes of high-density fluid rising from the inner wall. However, in the case of Boussinesq approximation, enhanced mixing can be observed in the core of the cavity with wider convection cells filling the region between hot and the cold walls, which augment the overall heat transfer rate between the outer and the inner walls of the cavity. This could be the possible reason for the overprediction of the Nusselt number in the case of incompressible calculations with the Boussinesq approximation.

Conclusions

A compressible code is used to study a centrifugal buoyancy induced flow in a closed rotating cavity for the Ra in the range of 10^6 to 10^8 for conditions matching the experimental conditions of Bohn et al. [1]. The comparison of Nu at the outer wall shows good agreement with experimental data for low Ra . At $Ra = 10^8$, a high value of Nu is predicted compared to the experimental value. The present study shows the well-defined flow structure in the domain with counter-rotating vortices analogous to Rayleigh-Bénard convection. The number of these counter-rotating convection rolls are different at the different values of Ra . The average temperature profiles comprise of an isothermal fluid core with two thermal boundary layers formed at the outer and inner cylindrical walls, whose thickness drop with the increase in the Ra . The comparison with the predictions of an

incompressible solver using Boussinesq approximation shows the overprediction of the Nu as compared to the results of the present study. Further, the comparison of the averaged temperature profiles show a deviation near the wall as well as in the core region of the cavity. The cause of this difference could be due to the Boussinesq approximation which considers the density as a linear function of temperature. Qualitative comparison of density contours obtained from the results of compressible code with the ones obtained from the Boussinesq approximation is reported. More uniform prediction of density by using Boussinesq approximation could be a reason behind the overprediction of the Nu in the latter case. However, this is still an open research question which requires further investigation by comparing the results of compressible and incompressible codes in more detail.

Acknowledgements

This work was supported by resources provided by the Pawsey Supercomputing Centre with funding from the Australian Government and the Government of Western Australia.

References

- [1] Bohn, D., Deuker, E., Emunds, R. and Gorzelitz, V., Experimental and theoretical investigations of heat transfer in closed gas-filled rotating annuli.
- [2] Grossmann, S., Lohse, D. and Sun, C., High-Reynolds number Taylor-Couette turbulence, *Annual review of fluid mechanics*, **48**, 2016, 53–80.
- [3] Hollands, K., Raithby, G. and Konicek, L., Correlation equations for free convection heat transfer in horizontal layers of air and water, *International Journal of Heat and Mass Transfer*, **18**, 1975, 879–884.
- [4] King, M. P., Wilson, M. and Owen, J. M., Rayleigh-Bénard convection in open and closed rotating cavities, *Journal of engineering for gas turbines and power*, **129**, 2007, 305–311.
- [5] Lopez, J. M., Marques, F. and Avila, M., The Boussinesq approximation in rapidly rotating flows, *Journal of Fluid Mechanics*, **737**, 2013, 56–77.
- [6] Pitz, D., Chew, J. and Marxen, O., Large-eddy simulation of buoyancy-induced flow in a sealed rotating cavity, *Proceedings of ASME Turbo Expo 2018*.
- [7] Pitz, D. B., Chew, J. W., Marxen, O. and Hills, N. J., Direct numerical simulation of rotating cavity flows using a spectral element-Fourier method, *Journal of Engineering for Gas Turbines and Power*, **139**, 2017, 072602.
- [8] Sandberg, R., Compressible-flow DNS with application to airfoil noise, *Flow, Turbulence and Combustion*, **95**, 2015, 211–229.
- [9] Sun, Z., Kilfoil, A., Chew, J. W. and Hills, N. J., Numerical simulation of natural convection in stationary and rotating cavities, *ASME Paper No. GT2004-53528*.